Artificial Fish Swarm Algorithm with Deep Learning Model for Content based Image Retrial and Classification on Retinal Fundus Images

[1]S. Syed Mahamood Shazuli, [2]A. Saravanan

[1]Research Scholar, Department of Computer and Information Sciences, Annamalai University.
[2]Assistant Professor/Programmer, Department of Computer and Information Sciences, Annamalai University.

Abstract

Retinal fundus images offer essential diagnostic data regarding different eye diseases, which include glaucoma, diabetic retinopathy (DR), and macular degeneration. In terms of retinal images, image retrieval is used to search for images that display similar patterns or characteristics like the severity of a specific disease or the presence of certain lesions. On the other hand, Classification is the process of allocating a category or label to an image related to its characteristics or features. Utilizing several methods, both image retrieval and classification of retinal fundus images are carried out, some of them are conventional deep learning (DL) ML techniques, and convolutional neural networks (CNNs). This study introduces an Artificial Fish Swarm Algorithm with Deep Learning Model for Content based Image Retrial and Classification on Retinal Fundus Images (AFSADL-IRC) technique. The presented AFSADL-IRC technique retrieves the fundus images and classifies them using DL model. To attain this, Guided filtering (GF) based pre-processing is applied for noise removal process. Next, the EfficientNet model produces a collection of feature vectors with AFSA based hyperparameter optimizer. To retrieve images, Manhattan Distance metric is used for similarity measurement. Finally, Elman neural network (ENN) model classifies the retrieved images into various classes. The experimental result analysis of the AFSADL-IRC algorithm is tested on retinal fundus image dataset and the outcomes indicate the better performance of the AFSADL-IRC technique compared to existing techniques.

Keywords: Image retrieval; Diabetic retinopathy; Image classification; Retinal fundus images; Elman neural network

1. Introduction

The internal surface of the eye, which is opposite to the focal point, is called as fundus [1]. It includes the vulnerable side/ optic plate, the retina, the fovea, the back shaft, and the macula. Fundus retinal structure is core microcirculation structure seen by non-intrusive approaches in the vascular structure [2]. For pathology determination, retinal fundus images offer a non-obtrusive symptomatic approach. Fundus image is a

significant clinical reason to know the condition of eye [3]. They were the main source for ophthalmologists in the segmentation process of the anatomical structure of the retina viz., macula, blood vessels, fovea, and optic disc for detecting the eye pathologies relevant to the retina. Glaucoma, Cataracts, conjunctivitis, and DRare common eye diseases that lead to blindness in humans [4]. A system that searches retrieves similar imageries, and browses the query images from huge datasets is termed Content Based Image Retrieval (CBIR). It has enabled users to query and relevant to the image extracted attributes [5], taking place based on automatically derived primitive features such as shapes, texture, spatial relation, and colour between objects.

CBIR based solutions are explored for making development in the diagnosis process, which will be helpful in medical imaging solutions [6]. CBIR endeavoured to diagnose retinal diseases using large dataset. Earlier research works utilized several imaging approaches such as ultrasonic images, retinal images [7], slit-lamp images and retro-illumination images for classifying and detecting cataracts. Of these, the commonly used images for the diagnosis of cataract is retinal. The classical techniques make an extraction process of handcrafted features and implement ML approaches for classifying cataracts [8]. The hand-crafted features like histogram of gradient (HoG), wavelet, colour, sketch features and texture determines the performance of these approaches. The manual feature selection and extraction require professional ophthalmologists' profound experience in the field and consume more time [9]. For cognitive waveform speech recognition, natural language processing and image classification etc., the most broadly used algorithm is Deep learning (DL) approaches like a convolutional neural network (CNN) [10]. Different from old ML approaches, CNN made an automatic extraction of the feature from images without human involvement.

This study introduces an Artificial Fish Swarm Algorithm with Deep Learning Model for Content based Image Retrial and Classification on Retinal Fundus Images (AFSADL-IRC) technique. The presented AFSADL-IRC technique retrieves the fundus images and classifies them using DL model. To attain this, Guided filtering (GF) based pre-processing is applied for noise removal process. Next, the EfficientNet model produces a collection of feature vectors with AFSA based hyperparameter optimizer. To retrieve images, Manhattan Distance metric is used for similarity measurement. Finally, Elman neural network (ENN) model classifies the retrieved images into various classes. The experimental results of the AFSADL-IRC technique are tested on retinal fundus image dataset.

2. Related Works

In [11], the authors enrich the quality of the input image identifies DME and DR in an initial stage by carrying out pre-processing including 3 steps: contrast enhancement, noise filtering, and artefact removal. Then, with Improved Mask-Regional CNN (Mask RCNN), blood vessel segmentation is performed, which leads to higher precision and accuracy rate of DME and DR detection. Lastly, classification and feature extraction utilizing VGG-16 is done, which abstracts orientation features, structural features, and colour. A new structure for DR classification and detection was designed in [12]. The image pre-processing was executed initially, and, by making use of the Multi threshold-based Remora Optimization (MTRO) technique, vessel segmentation has been carried out. Through Wild Geese Algorithm (WGA) and Region-based CNN (R-CNN), the classification

and feature extraction are effectuated. Fang and Qiao [13] a new DAG network method depends on multi-feature fusion of retinal images is offered for classifying DR. Depends on a new DAG network, three features are transferred to a classification method to realize feature learning and multi-feature fusion. Eventually, to classify and recognize diabetic retinopathy, the optimized classification approach was used.

Sakaguchi et al. [14] devised a technique based on Graph Neural Network (GNN) to enrich exactness for severity classification. It encompasses of two features. The extraction of Region-Of-Interest (ROI) sub-images initially, concentrates on regions locally capturing lesions for diminishing background noises in image pre-processing for the classification. Aziza et al. [15] designed an automatic mechanism for detecting DR from color retinal images. The method depends on segmenting process of blood vessels and extracting the geometric features, applied in the initial identification of DR. The Hessian matrix, active contour and ISODATA method were applied for segmenting the blood vessels. At last, the authors have implemented the DT-CART technique for classifying images into normal (NO-DR) or DR.

3. The proposed model

In this study, we have introduced a new AFSADL-IRC technique for the retrieval and classification of fundus images. The presented AFSADL-IRC technique retrieves the fundus images and classifies them using DL model. It comprises GF based preprocessing, EfficientNet, AFSA based hyperparameter tuning, Manhattan distance-based similarity measurement, and ENN classification. Fig. 1 shows the workflow of AFSADL-IRC method.

A. *Image Pre-processing*

Here, the GF based pre-processing is exploited for noise removal process. The GF is a kind of non-linear filter that have used guidance images for filtering an input image [16]. The guidance image offers data regarding the image structure, and the filter with data smoothens the input images and preserving its edges. GF is expressed in form of linear filtering operation, which made it a potential one for computation purposes.
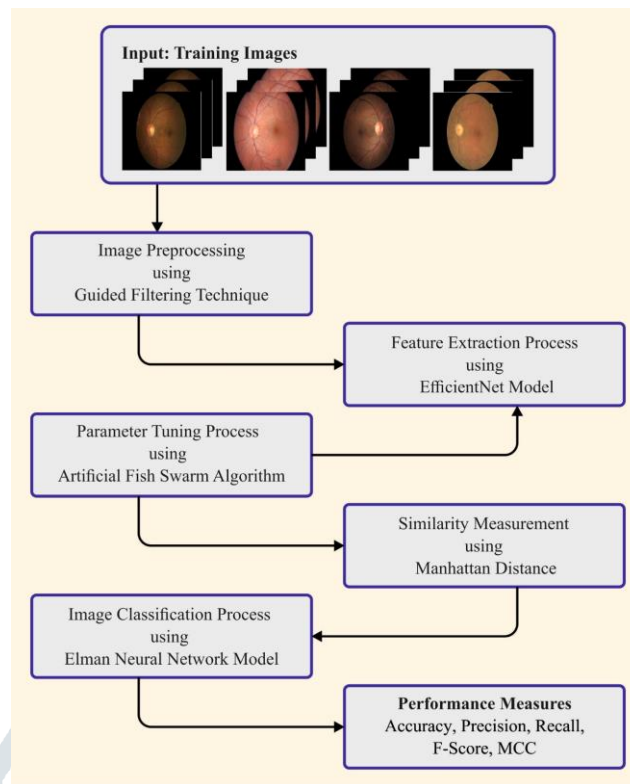
Fig. 1. Workflow of AFSADL-IRC approach

B. *Feature Extraction using EfficienNet*

In this work, the EfficientNet model produces a collection of feature vectors. EffcientNet is developed to increase the accuracy and efficiency of CNN by using a uniform scaling mechanism to all the dimensions viz., resolution, depth, and width of the network but still scaling down the model [17]. In general, ConvNet scales up or down by fluctuating the network resolution, width, or depth. But scaling individual dimensions of the network augments accuracy. Therefore, to accomplish the best efficiency and accuracy, it is significant to uniformly scale each dimension of network depth, width, and resolution. Fig. 2 depicts the structure of EffcientNet model.

Fig. 2. Structure of EffcientNet

The compound scaling method exploits grid search to determine the relations amongst the scaling dimension of the baseline network in fixed resource constraints. In the presented technique, an acceptable scaling feature for depth, width, and resolution dimension is defined. This coefficient was employed for scaling the baseline network to the desired target. This kind of structure is named the EfficientNet model and it has 8 dissimilar variations between EfficientNet B0-B7. As the model count rises, the efficiency of EfficientNet rises explicitly. They were named EfficientNet since they accomplish best efficiency and accuracy than the prior CNN.

The poential block of the EfficientNet family is the inverted bottleneck MBConv that is based on the MobileNetV2 model. MBconv block was an inverted residual block that encompasses layers that firstly widen and expand the channel, so the direct connection is utilized between bottlenecks that intersect a less volume of channels than the expansion layer. Additionally, this framework employs in-depth separable convolution that

brings down computation by approximately a k^2 factor than normal layers whereas k represents kernel size. For working with inverted residual connection and to enhance accuracy, a novel activation function termed Swish activation was utilized rather than the $ReLu$ activation function. To construct the variant of baseline models, distinct values will be replaced for the compound coefficient psi.

$$Depth: d = \alpha\psi \tag{1}$$

$$Width: w = \beta\psi \tag{2}$$

$$resolution: r = \gamma\psi \tag{3}$$

$$\alpha \geq 1, \beta \geq 1, \gamma \geq 1$$

Whereas α, β, γ denotes constant fixed through grid search and define how to allot this extra resource to the resolution, width, and depth of the network correspondingly, ψ represents user-determined coefficients which control how much resources are available for model scaling.

C. Hyperparameter Tuning using AFSA

The AFSA is applied for the hyperparameter tuning process. The AFSA mimics the grouping, rear-end, and foraging behaviours of fish swarming by creating artificial fish (AF) swarming and adopts a bottom-up optimization technique to begin from natural behaviours of making individuals, ascertain behaviours of the highest food density in space [18]. The external insight of AF can be accomplished by relying on virtual vision, and the subsequent method was used for achieving a virtual vision of AF:

$$X_v = X + Visuanl \times Rand(\ ) \tag{4}$$

$$X_{next} = X + X_V - X\|X_V - X\| \times Step \times Rand(\ ) \tag{5}$$

From the expression, $Step$ denotes a step size, and $Rand()$ is a random operator used for generating random integer within [0,1]. The four behaviours of AF are briefly described in the following:

Foraging behavior: generally, it is assumed that food concentration or sense food of fish in water through taste or virtual vision to select the direction of actions. Set state of existing AF, and randomly choose additional state in its visual range. When the objective function of the attained state was greater than the recent state, it moves go a step further to the last state; if not, it reselects the novel state. Eq. (6) defines that the AF X_i arbitrarily chooses a state X_j in its virtual vision

$$X_j = X_i + Visuanl \times Rand(\ ) \tag{6}$$

Compute the value of objective function Y_i and Y_j of X_i and X_j correspondingly, If Y_j is found to be more efficient than Y_i, then X_i move one step towards the X_j:

$$X_i^{t+1} = X_i^t + \frac{X_j - X_i^t}{||X_j - X_i^t||} \times Step \times Rand(\ ) \tag{7}$$

or else, X_i continue to choose the state X_j in its virtual vision, decide either the criteria are satisfied, and if still not stratified afterwards the frequent attempts of $try\_$number, perform an arbitrary behavior.

Group behavior: Algorithm 2 demonstrates the pseudocode snippets for the group behavior. In the present neighborhood, the AF explored the number of partners, computes the centre location of the partner, and later

compare the new objective function of central location with the main function of present location. When fish flock together, three rules should be observed: firstly, try moving towards the center of neighboring partner; next, avoid overcrowding and then, try to be consistent with average direction of neighboring partner. The AF X_i find the count of partners and the central location X_c in the present visual vision ($d_{ij} < visual$), if $\frac{Y_C}{nf} < \delta \times Y_i$ (where Y_C and Y_i denotes the fitness value of X_c and X_i, correspondingly), it specifies that the central location of partners is less crowded and more efficient, and X_i move further step towards the central location of partners:

$$X_i^{t+1} = X_i^t + \frac{X_j - X_i^t}{||X_j - X_i^t||} \times Step \times Rand(\ ) \tag{8}$$

Or else, the foraging behaviour will be implemented.

Rear-end behavior: Algorithm 3 demonstrates the pseudocode snippet for the Rear-end behaviour. It characterizes the fish's behaviour to move in the optimum direction within its virtual vision. The AF X_i find individual X_j with the maximum fitness in its view ($d\_ij < visual$), and fitness value was Y_j, and explore count of partners in its view of the AF X_i, when $\frac{Y_j}{nf} < \delta \times Y_i$, representing that X_j is in a best state and was not crowded, X_i move further step toward X_j, if not it performs foraging behaviours.

Random behavior: it becomes the default behavior of foraging behavior, which represents the random movement of AF. If the food is found, it rapidly moves towards the increasing food. This is to discover partners or food points in a wide range.

$$X_i^{t+1} = X_i^t + Visuanl \times Rand() \tag{9}$$

Fitness selection is a crucial factor in the AFSA approach. Solution encoding is exploited for assessing the goodness of candidate solution. Now, the accuracy value is the main condition utilized for designing a fitness function.

$$Fitness = \max(P) \tag{10}$$

$$P = \frac{TP}{TP + FP} \tag{11}$$

Where FP denotes the false positive value and TP signifies the true positive from the expression.

D. Similarity Measure for Retrieval Process

To retrieve images, Manhattan Distance metric is used for similarity measurement. For all feature vectors and Manhattan distances, the adjacent N candidate images are added in a histogram of place [19]. By considering each query vector, to derive a list of N top-ranked candidate imageries, the resulting histogram has been utilized. The Manhattan distance is the differences lie in-between the two vectors and in 2D space, this can be represented in Eq. (12):

$$d = |p_1 - q_1| + |p_2 - q_2| \tag{12}$$

The Manhattan distance for q_i and p_i data points were defined for n-dimensional space, as in Eq. (13):

$$d_n = \sum_{i=1}^{n} |p_i - q_i| \tag{13}$$

E. Image Classification

The ENN model classifies the retrieved images into various classes in the final stage. The traditional ENN grants the hidden nodes feedback. The output layer nods feedback is not considered. Thus, developed a IENN method which is an enhanced form of ENN using output-input feedback [20]. This technique adds feedback called context layer 2 from the output node. The hidden layer node receives data of input layer node, context layers 2 and 1 nodes and it can be modelled mathematically in the equation:

$$\begin{cases} x(k) = f\big(w^3 x_c(k) + w^1 u(k-1) + w^4 y_c(k)\big) \\ x_c(k) = \alpha x_c(k-1) + x(k-1) \\ y_c(k) = \gamma x_c(k-1) + y(k-1) \\ y(k) = g\big(w^2 x(k)\big) \end{cases} \tag{14}$$

Here, γ indicates self-connected feedback gain factor; represents activation function in the output layer, w^3 and w^4 signify the connection weight of 1 and 2 context layers to the hidden layers, b^3 and b^4 refers to the threshold of 1 and 2 context layers, $f(\cdot)$ signifies activation function in hidden layer, g is given below.

$$f(x) = \frac{1}{1 + e^{-x}} \tag{15}$$

$$g(x) = x \tag{16}$$

With the use of gradient network model, IENN model can be achieved. The IENN objective function (error function) was expressed.

$$E(k) = \frac{1}{2}[y(k) - y]^T [y(k) - y] \tag{17}$$

The actual output was signified as *y* in Eq. (17).

4. Results and Discussion

The retrieval and classification outcomes of the AFSADL-IRC technique are investigated using a set of retinal fundus images. Fig. 3 exemplifies the sample query and retrieved images.
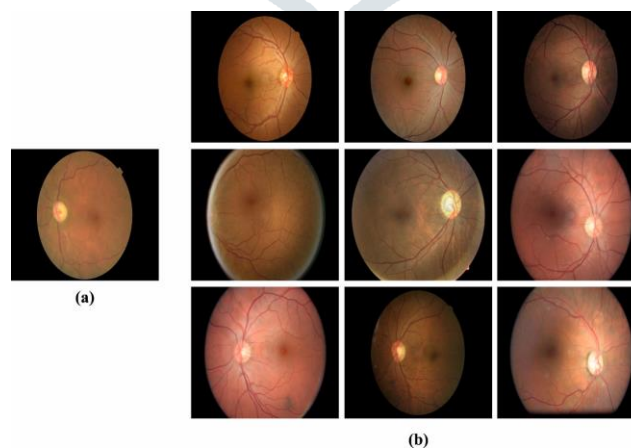

Fig. 3. a) Query Image b) Retrieved Images

Table 1 presents the overall classification results of the AFSADL-IRC technique.

In Fig. 4, the $accu_y$, $prec_n$, and $reca_l$ study of the AFSADL-IRC approach is provided clearly. The results pointed out that the AFSADL-IRC method reaches effectual outcomes under all classes. On entire dataset, the AFSADL-IRC approach reaches average $accu_y$, $prec_n$, and $reca_l$ of 98.78%, 92.60%, and 86.66% respectively. In the meantime, on 70% of TRP, the AFSADL-IRC method reaches average $accu_y$, $prec_n$, and $reca_l$ of 98.76%, 92.85%, and 86.33% correspondingly. Eventually, on 30% of TSP, the AFSADL-IRC method reaches average $accu_y$, $prec_n$, and $reca_l$ of 98.84%, 92.01%, and 87.47% respectively.

In Fig. 5, the F_{score} and MCC study of the AFSADL-IRC technique is provided clearly. The results indicate that the AFSADL-IRC technique reaches effectual outcomes under all classes. On entire dataset, the AFSADL-IRC technique reaches average F_{score} and MCC of 89.38% and 88.25% respectively. Meanwhile, on 70% of TRP, the AFSADL-IRC technique reaches average F_{score} and MCC of 89.28% and 88.17% correspondingly. Eventually, on 30% of TSP, the AFSADL-IRC approach reaches average F_{score} and MCC of 89.62% and 88.46% correspondingly.

Fig. 6 inspects the accuracy of the AFSADL-IRC method during the training and validation process on test dataset. The figure notifies that the AFSADL-IRC technique reaches increasing accuracy values over increasing epochs. Further, the increasing validation accuracy over training accuracy revealed that the AFSADL-IRC method learns efficiently on the test dataset.

TABLE I

CLASSIFIER OUTCOME OF AFSADL-IRC APPROACH WITH DISTINCT CLASSES

Class	$Accu_y$	$Prec_n$	$Reca_l$	F_{score}	MCC
Entire Dataset					
No DR	97.82	97.86	99.21	98.53	94.38
Mild DR	99.05	94.18	92.06	93.11	92.60
Moderate DR	98.71	96.15	95.24	95.69	94.93
Severe DR	99.10	87.60	74.46	80.50	80.32
Proliferative DR	99.23	87.22	72.32	79.07	79.04
Average	**98.78**	**92.60**	**86.66**	**89.38**	**88.25**
Training Phase (70%)					
No DR	97.80	97.82	99.22	98.51	94.36
Mild DR	99.02	93.67	92.01	92.83	92.31
Moderate DR	98.66	95.94	95.25	95.59	94.80
Severe DR	99.10	88.53	74.08	80.66	80.54
Proliferative DR	99.21	88.29	71.12	78.78	78.86
Average	**98.76**	**92.85**	**86.33**	**89.28**	**88.17**
Testing Phase (30%)					

No DR	97.86	97.95	99.19	98.57	94.42
Mild DR	99.12	95.34	92.18	93.73	93.27
Moderate DR	98.81	96.65	95.21	95.93	95.24
Severe DR	99.12	85.39	75.40	80.09	79.80
Proliferative DR	99.28	84.75	75.38	79.79	79.56
Average	**98.84**	**92.01**	**87.47**	**89.62**	**88.46**
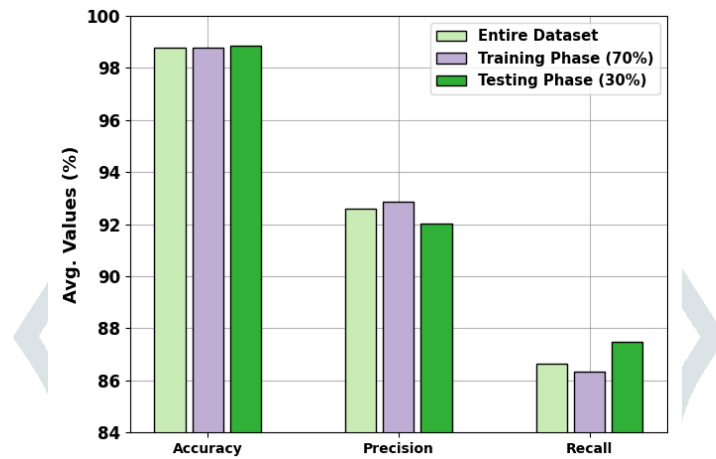
Fig. 4. Average outcome of AFSADL-IRC approach in terms of $accu_y$, $prec_n$, and $reca_l$
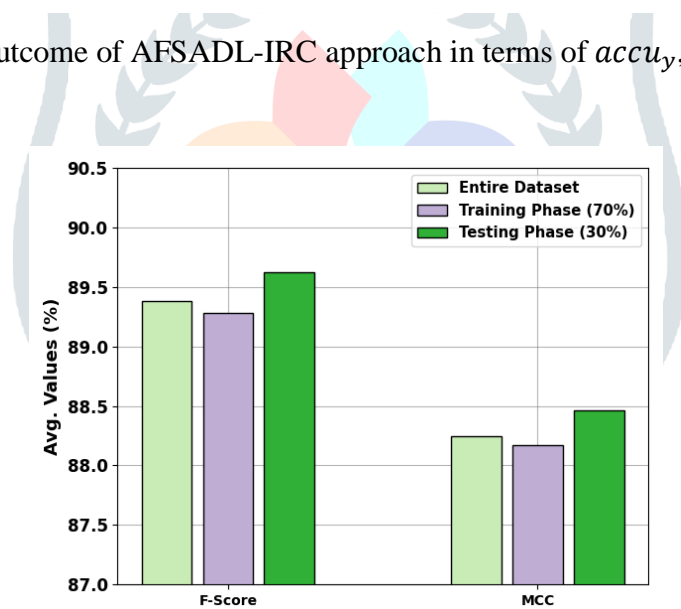

Fig. 5. Average outcome of AFSADL-IRC approach in terms of F_{score} and MCC

Fig. 6. Accuracy curve of AFSADL-IRC approach

The loss analysis of the AFSADL-IRC approach at the time of training and validation is demonstrated on the test dataset in Fig. 7. The results indicate that the AFSADL-IRC method reaches closer values of training and validation loss. It is observed that the AFSADL-IRC technique learns efficiently on the test dataset.

A brief precision-recall (PR) curve of the AFSADL-IRC technique is shown on the test dataset in Fig. 8. The results stated that the AFSADL-IRC technique has increasing values of PR. Also, the AFSADL-IRC method can reach greater PR values in all classes.
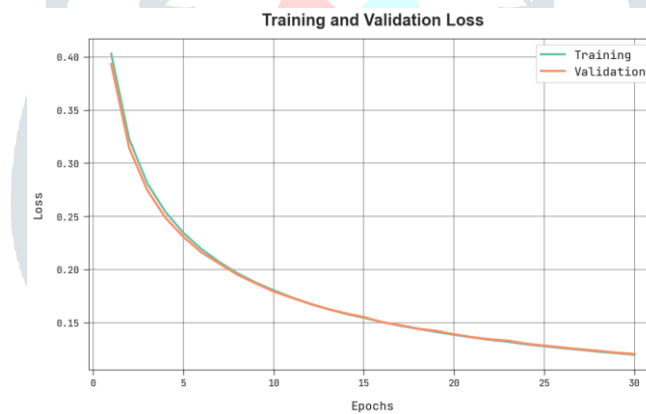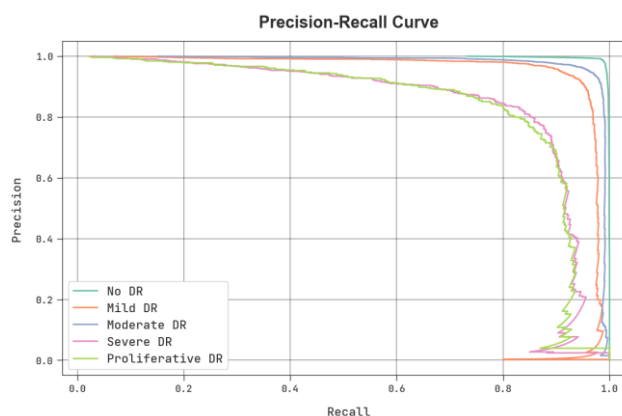

Fig. 7. Loss curve of AFSADL-IRC approach

Fig. 8. Precision-recall curve of AFSADL-IRC approach

TABLE 2

ACCURACY ANALYSIS OF AFSADL-IRC ALGORITHM WITH RECENT APPROACHES

Methods	Accuracy (%)
AFSADL-IRC	98.84
WFDLN	98.00
AlexNet	89.50
MobileNet	92.90
Xception	92.80
ResNet-50	94.51

In Table 2 and Fig. 9, a widespread $accu_y$ inspection of the AFSADL-IRC technique is made with recent models. The results demonstrate that the AlexNet model leads to worse outcomes while the MobileNet and Xception models attain closer performance. Although the ResNet-50 reaches $accu_y$ of 94.51%, the WFDLN model results in certainly better $accu_y$ of 98%. But the AFSADL-IRC technique outperforms the other models with maximum $accu_y$ of 98.84%. Therefore, the AFSADL-IRC technique appeared as an effectual tool for fundus image retrieval and classification.
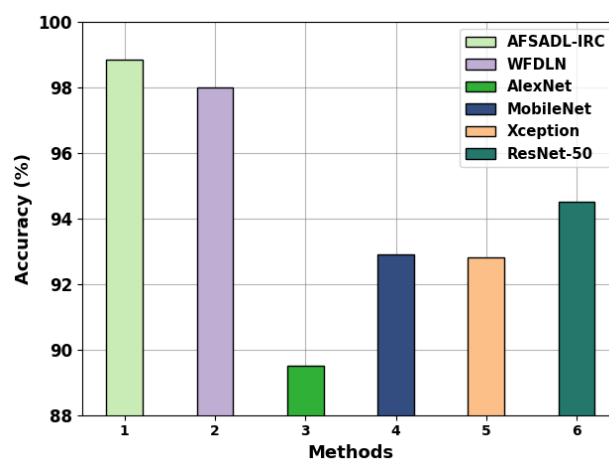

Fig. 9. Accuracy analysis of AFSADL-IRC algorithm with recent approaches

5. Conclusion

In this article, we have introduced a new AFSADL-IRC algorithm for the retrieval and classification of fundus images. The presented AFSADL-IRC method retrieves the fundus images and classif them using DL model. It comprises GF based preprocessing, EfficientNet, AFSA based hyperparameter tuning, Manhattan distance-based similarity measurement, and ENN classification. In this work, the EfficientNet model produces a collection of feature vectors with AFSA based hyperparameter optimizer. To retrieve images, Manhattan Distance metric is used for similarity measurement. Finally, the ENN model classifies the retrieved images into various classes. The experimental result of the AFSADL-IRC approach is tested on retinal fundus image dataset

and the results indicate the superior performance of the AFSADL-IRC algorithm than existing techniques. In upcoming years, the performance of the AFSADL-IRC method can be boosted by deep instance segmentation process.

REFERENCES

[1] Pragathi, P. and Rao, A.N., 2022. An effective integrated machine learning approach for detecting diabetic retinopathy. *Open Computer Science*, *12*(1), pp.83-91.

[2] Khan, S.H., Abbas, Z. and Rizvi, S.D., 2019, February. Classification of diabetic retinopathy images based on customised CNN architecture. In *2019 Amity International conference on artificial intelligence (AICAI)* (pp. 244-248). IEEE.

[3] Reddy, G.T., Bhattacharya, S., Ramakrishnan, S.S., Chowdhary, C.L., Hakak, S., Kaluri, R. and Reddy, M.P.K., 2020, February. An ensemble based machine learning model for diabetic retinopathy classification. In *2020 international conference on emerging trends in information technology and engineering (ic-ETITE)* (pp. 1-6). IEEE.

[4] Lavanya, S., and P. Naveen. "Detection of Retinal Neovascularization Using Optimized Deep Convolutional Neural Networks." Journal of Trends in Computer Science and Smart Technology 4, no. 1 (2022): 38-49.

[5] Parthasharathi, G. U., R. Premnivas, and K. Jasmine. "Diabetic Retinopathy Detection Using Machine Learning." Journal of Innovative Image Processing 4, no. 1 (2022): 26-33.

[6] Dayana, A.M. and Emmanuel, W.R., 2022. An enhanced swarm optimization-based deep neural network for diabetic retinopathy classification in fundus images. *Multimedia Tools and Applications*, pp.1-32.

[7] Ragab, M., Aljedaibi, W.H., Nahhas, A.F. and Alzahrani, I.R., 2022. Computer aided diagnosis of diabetic retinopathy grading using spiking neural network. *Computers and Electrical Engineering*, *101*, p.108014.

[8] Qomariah, D.U.N., Tjandrasa, H. and Fatichah, C., 2019, July. Classification of diabetic retinopathy and normal retinal images using CNN and SVM. In *2019 12th International Conference on Information & Communication Technology and System (ICTS)* (pp. 152-157). IEEE.

[9] Dayana, A.M. and Emmanuel, W.R., 2022. Deep learning enabled optimized feature selection and classification for grading diabetic retinopathy severity in the fundus image. *Neural Computing and Applications*, pp.1-21.

[10] Elwin, J.G.R., Mandala, J., Maram, B. and Kumar, R.R., 2022. Ar-HGSO: Autoregressive-Henry Gas Sailfish Optimization enabled deep learning model for diabetic retinopathy detection and severity level classification. *Biomedical Signal Processing and Control*, *77*, p.103712.

[11] Nage, P., Shitole, S. and Kokare, M., 2023. An intelligent approach for detection and grading of diabetic retinopathy and diabetic macular edema using retinal images. *Computer Methods in Biomechanics and Biomedical Engineering: Imaging & Visualization*, pp.1-16.

[12] Vinayaki, V.D. and Kalaiselvi, R., 2022. Multithreshold image segmentation technique using remora optimization algorithm for diabetic retinopathy detection from fundus images. *Neural Processing Letters*, *54*(3), pp.2363-2384.

[13] Fang, L. and Qiao, H., 2022. Diabetic retinopathy classification using a novel DAG network based on multi-feature of fundus images. *Biomedical Signal Processing and Control*, *77*, p.103810.

[14] Sakaguchi, A., Wu, R. and Kamata, S.I., 2019, March. Fundus image classification for diabetic retinopathy using disease severity grading. In *Proceedings of the 2019 9th international conference on biomedical engineering and technology* (pp. 190-196).

[15] Aziza, E.Z., El Amine, L.M., Mohamed, M. and Abdelhafid, B., 2019, November. Decision tree CART algorithm for diabetic retinopathy classification. In *2019 6th International Conference on Image and Signal Processing and their Applications (ISPA)* (pp. 1-5). IEEE.

[16] Stimpel, B., Syben, C., Schirrmacher, F., Hoelter, P., Dörfler, A. and Maier, A., 2019. Multi-modal deep guided filtering for comprehensible medical image processing. *IEEE transactions on medical imaging*, *39*(5), pp.1703-1711.

[17] Zheng, B., Gao, A., Huang, X., Li, Y., Liang, D. and Long, X., 2023. A modified 3D EfficientNet for the classification of Alzheimer's disease using structural magnetic resonance images. *IET Image Processing*, *17*(1), pp.77-87.

[18] Zhu, Y., Wang, C., Sun, J. and Yu, F., 2023. A Chaotic Image Encryption Method Based on the Artificial Fish Swarms Algorithm and the DNA Coding. *Mathematics*, *11*(3), p.767.

[19] Shazuli, S.S.M. and Saravanan, A., 2022, December. Retinal Fundus Image Retrieval and Classification using Optimal Deep Learning Model. In *2022 International Conference on Automation, Computing and Renewable Systems (ICACRS)* (pp. 639-645). IEEE.

[20] Islam, N. and Irshad, K., 2022. Artificial ecosystem optimization with Deep Learning Enabled Water Quality Prediction and Classification model. *Chemosphere*, *309*, p.136615.